Received: 7 December 2020 | Revised: 21 April 2021 | Accepted: 5 May 2021

IET Microwaves, Antennas & Propagation

DOI: 10.1049/mia2.12138

The Institution of Engineering and Technology WILEY

ORIGINAL RESEARCH PAPER

Flexible ultra-high transformation ratio-based dual-band impedance transformer and its applications in a T-junction power divider

Deepayan Banerjee[1] | **Mohammad Hashmi**[2] | **Fadhel Ghannouchi**[3]

[1]Dept. of Electronics and Communication Engineering, IIIT Delhi, New Delhi, India

[2]School of Engineering and Digital Sciences, Nazarbayev University, Nur Sultan, Kazakhstan

[3]Dept. of Electrical and Computer Engineering, University of Calgary, Alberta, Canada

Correspondence

Mohammad Hashmi, School of Engineering and Digital Sciences, Nazarbayev University, Nur Sultan, 010000, Kazakhstan.
Email: mohammad.hashmi@nu.edu.kz

Funding information

Nazarbayev University, Grant/Award Number: 021220CRP0222

Abstract

A design scheme is presented for an all-pass coupled-line (APCL)-based dual-band impedance-matching network. Salient features include a highly flexible frequency ratio (r) (high of 15 and low of 1.2) and impedance transformation ratio (k) (high of 9 and low of 0.2) simultaneously at two arbitrary, uncorrelated frequencies of interest. The design strategy consists of two APCL sections and a stub that prove to be simple and easy to prototype. Detailed mathematical modelling and graphical interpretations have been presented. Closed-form design equations have been developed and backed up with design examples. Two dual-band T-junction power dividers (TPDs) have been designed to demonstrate the application of the proposed impedance transformer at two widely separated frequencies. RO4350 B- and RO5880-based prototypes have been fabricated for both the matching network and the TPD to validate the proposed theory. The measurement results demonstrate an achievable frequency ratio of 15 and an impedance transformation ratio of 9 in simultaneous operation mode.

1 | INTRODUCTION

The last decade has seen a huge upsurge in the development of wireless communication devices. Their utility has drastically simplified human lives with applications including mobile telephony, broadcasting and entertainment, military and space applications, and medical instrumentation. Impedance-matching networks are one of the key elements of all electronic systems. From the perspective of RF and microwave circuits, impedance transformers are essential for maximum power transfer between connected modules. They find application in a broad range of passive and active devices such as power dividers, couplers, crossovers, mixers, and amplifiers.

The pressing needs of emerging wireless applications over the years have directed considerable research to multiband devices. The existing literature is replete with dual-band impedance transformer architectures [1–21], but most of them have fundamental limitations, namely, a lower frequency ratio (r) and impedance transformation ratio (k) [3–10]. The well-known Monzon transformer [2] theoretically allows very high values for the frequency and impedance transformation ratios, but the obtained design parameters become highly restricted because of fabrication limits. Few architectures [10, 13, 14] have utilised additional short/open stubs to mitigate transformation ratio limitations, the role of which is to introduce extra transmission zeros in addition to impedance matching. Another impedance transformer, reported in [16], utilises a dual-transmission line approach to achieve high transformation ratio values. However, these designs cannot "push their limits" as the line impedances acquire unrealisable values. A slow-wave-structure-based dual-band impedance transformer has been proposed in [19] that matches real load and source impedances at two arbitrary frequencies of interest. The transformation ratios are limited by the line separation of C-section coupled lines, which tend to achieve unrealisable values on extension. A coupled line cascaded with planar transmission line architecture has been reported in [20]. The proposed design facilitates an impedance transformation ratio range from 0.1 till 10 at frequency ratios between 2 and 7. The circuit is limited by its non-simultaneous behaviour in which

improvement of one transformation ratio (frequency or impedance) degrades the other.

With the recent advancement of wireless standards and the increase in the number of devices using the radio spectrum, there has been an abrupt broadening of the spectrum in which these devices operate. As a result, for a dual-band device, the two frequencies of operation might be widely separated. A majority of the architectures discussed above operate at lower frequency and impedance transformation ratios. An early report [11] has addressed the case of improving the impedance transformation ratio but only for single-band operation. Recently [21], a cross-coupled architecture for impedance transformers capable of handling extreme load values was reported. The design claims an impedance transformation ratio of 0.1 to 40 but only for single-band operation with moderate design flexibility. A comprehensive analysis on the simultaneous extension of both the frequency and the impedance transformation ratio for dual-band matching networks is thus lacking.

This article investigates the role of a "floating-arm" type all-pass coupled-line (APCL) in transformation ratio extension. This configuration is of particular interest because of its relaxed design constraints for selecting line impedances that are otherwise not implementable using traditional transmission lines. In this regard, a novel dual-band impedance transformer using APCLs has been proposed. A rigorous analysis is performed, and a mathematical model has been developed that demonstrates the possibility of expansion of the limits of the frequency ratio from 1.2 to 15 and the impedance transformation ratio from 0.2 to 9 simultaneously. The proposed theory is backed by simulation case studies and experimental results comprising fabricated prototypes and their measurements. As an application of the developed matching network, an equal-split T-junction power divider (TPD) has also been designed and fabricated with the same specifications. Measured results of the divider validate the design and highlight the utility of the proposed theory.

2 | PROPOSED IMPEDANCE TRANSFORMER

The architecture of the proposed dual-band impedance transformer is illustrated in Figure 1. The APCL [Z_{e1}, Z_{o1}, θ_1] transforms the real load Z_L into two complex-conjugate admittances, namely, $G_1 + jB_1$ and $G_1 - jB_1$ at f_1 and f_2 respectively. [$Z_{OC/SC}$, θ_S] is a dual-band stub that cancels the net susceptance $\mp(B_1 + B_2)$ generated from the load-side and the source-sided APCLs at the two frequencies. The stub may be either open or short circuit depending on the sign of the susceptance generated. After susceptance cancellation, the remaining equal-valued conductance G_1 at f_1 and f_2 is matched to the source Z_S by a similar APCL [Z_{e2}, Z_{o2}, θ_2]. The mathematical analysis and derivation of the design parameters are provided in the upcoming subsections.

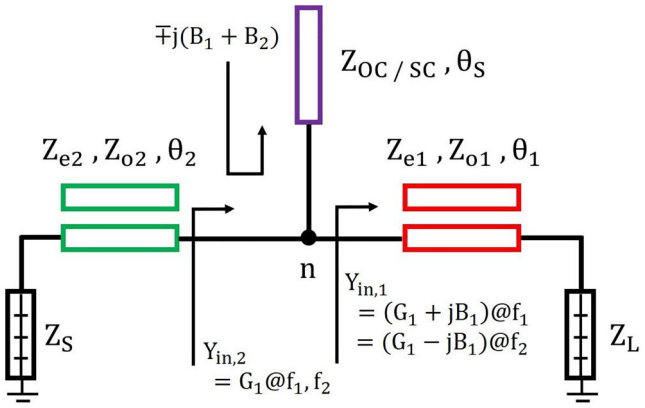

FIGURE 1 The proposed dual-band impedance transformer

2.1 | Complex-conjugate generator [Z_{e1}, Z_{o1}, θ_1]

Figure 2 illustrates the APCL structure with ports marked where Z_i is the image impedance. The Z parameters given in [1] for this architecture can be obtained by simple current-voltage analysis of the coupled line [22]. Furthermore, the image impedance Z_i of the APCL structure is expressed in Equation (2). Equations (1) and (2) can be simplified to obtain the expression of Z_i given in Equation (3).

$$Z_{11} = Z_{44} = \frac{-j}{2}(Z_{e1} + Z_{o1})\cot\theta_1 \tag{1a}$$

$$Z_{14} = Z_{41} = \frac{-j}{2}(Z_{e1} + Z_{o1})\csc\theta_1 \tag{1b}$$

$$Z_i = \sqrt{Z_{11}^2 - \frac{Z_{11}Z_{14}^2}{Z_{44}}} \tag{2}$$

$$Z_i = \frac{Z_{e1} + Z_{o1}}{2} \tag{3}$$

For complex-conjugate generation at f_1 and f_2, the condition in Equation (4) must be satisfied. Further simplification gives the expression for Z_{e1} in Equation (5). Apparently, the value of Z_{o1} within the fabricable limits of [20 − 160] Ω enables the determination of Z_{e1}. It must be noted that the values of Z_{e1} and Z_{o1} should be close to each other under the condition $Z_{o1} < Z_{e1}$ for the APCL sections to be fabricable. The ABCD parameters are obtained from the transformation relation in Equation (6) and are expressed in Equation (7).

$$\frac{Z_{e1} + Z_{o1}}{2} = \sqrt{Z_S Z_L} \tag{4}$$

$$Z_{e1} = 2\sqrt{Z_S Z_L} - Z_{o1} \tag{5}$$

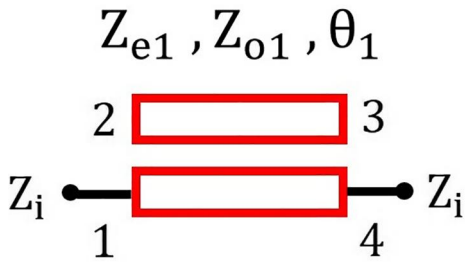

FIGURE 2 All-pass coupled line in floating-arm configuration

$$\begin{bmatrix} A & B \\ C & D \end{bmatrix} = \begin{bmatrix} Z_{11}/Z_{41} & (Z_{11}Z_{44} - Z_{14}Z_{41})/Z_{41} \\ 1/Z_{41} & Z_{44}/Z_{41} \end{bmatrix} \quad (6)$$

$$\begin{bmatrix} A & B \\ C & D \end{bmatrix} = \begin{bmatrix} \left(\frac{Z_{e1}+Z_{o1}}{Z_{e1}-Z_{o1}}\right)\cos\theta_1 & \frac{j}{2}(Z_{e1}+Z_{o1})\sin\theta_1 \\ \frac{2j\sin\theta_1}{(Z_{e1}+Z_{o1})} & \left(\frac{Z_{e1}+Z_{o1}}{Z_{e1}-Z_{o1}}\right)\cos\theta_1 \end{bmatrix} \quad (7)$$

The admittance $Y_{in,1}$ obtained after the load-side APCL stage can be expressed in Equation (8). Now, $Y_{in,1}$ in Equation (9) can be obtained by simplifying Equations (7) and (8):

$$Y_{in,1} = \frac{CZ_L + D}{AZ_L + B} \quad (8)$$

$$Y_{in,1} = \frac{\frac{(Z_{e1}nm + Z_{o1})\cos\theta_1}{Z_{e1}-Z_{o1}} + \frac{2jZ_L\sin\theta_1}{Z_{e1}+Z_{o1}}}{\frac{j}{2}(Z_{e1}+Z_{o1})\sin\theta_1 + \frac{Z_L(Z_{e1}+Z_{o1})\cos\theta_1}{Z_{e1}-Z_{o1}}} \quad (9)$$

Decomposing Equation (9) into real and imaginary parts, $Y_{in,1} = G_1 \pm jB_1$ at f_1 and f_2, respectively, can be obtained in (2.1), the values of which are easily obtained using MATLAB:

$$G_1 = \frac{Z_L\cos^2\theta_1(Z_{e1}+Z_{o1})^2}{(Z_{e1}-Z_{o1})^2\sigma} + \frac{Z_L(Z_{e1}+Z_{o1})\sin^2\theta_1}{(Z_{e1}+Z_{o1})\sigma} \quad (10a)$$

$$B_1 = \frac{2Z_L^2\sin\theta_1\cos\theta_1 - \frac{1}{2}(Z_{e1}+Z_{o1})^2\sin\theta_1\cos\theta_1}{\rho} \quad (10b)$$

where

$$\sigma = \frac{1}{4}(Z_{e1}+Z_{o1})^2\sin^2\theta_1 + \frac{Z_L^2(Z_{e1}+Z_{o1})^2\cos^2\theta_1}{(Z_{e1}-Z_{o1})^2}$$

and

$$\rho = (Z_{e1}-Z_{o1})\left[\frac{1}{4}(Z_{e1}+Z_{o1})^2\sin^2\theta_1 + \frac{Z_L^2(Z_{e1}+Z_{o1})^2\cos^2\theta_1}{(Z_{e1}-Z_{o1})^2}\right]$$

For dual-band operation at f_1 and f_2, let us consider electrical lengths at the respective frequencies to be θ and θ_1. Now, from the behaviour of transmission lines, $\theta + \theta_1 = n\pi$, where n is an integer. If $\theta = r\theta_1$ where, $r = f_2/f_1$, the expression reduces to $\theta_1 + r\theta_1 = n\pi$. This enables determination of the electrical length of the dual-band L-network in Equation (11). Here, $n \in [1, 2, 3\ldots)$.

$$\theta_1 = \frac{n\pi}{1+r} \quad (11)$$

The real part of the admittance, $\mathrm{Re}\{Y_{in,2}\} = G_1$ at both f_1 and f_2, is matched to Z_S by another (source-side) APCL section $[Z_{e2}, Z_{o2}, \theta_2]$.

2.2 | Conductance-matching line [Z_{e2}, Z_{o2}, θ_2]

For the line to operate as a dual-band quarter-wave transformer, the impedance condition in Equation (12) must be satisfied. The conditions in Equations (3) and (12) can be simplified to obtain the design parameters as expressed in (13). Here, $K = Z_{o2}/Z_{e2}$:

$$Z_i = \sqrt{\frac{Z_S}{G_1}} \quad (12)$$

$$Z_{e2} = \frac{2\sqrt{\frac{Z_S}{G_1}}}{1+K} \quad (13)$$

The susceptance generated by this section, B_2, can be calculated from Equation (10b) by replacing Z_L with Z_S and $[Z_{e1}, Z_{o1}, \theta_1]$ with $[Z_{e2}, Z_{o2}, \theta_2]$, where $\theta_2 = m\theta_1$ and $m \in [1, 2, 3\ldots)$.

2.3 | Dual-band susceptance cancellation stub

Susceptances B_1 and B_2 are added and cancelled using a dual-band susceptance cancellation stub, the parameters of which are expressed in (2.3). Here, OC and SC are for open circuit and short circuit stubs, respectively, and $\theta_S = p\theta_1$ where $p \in [1, 2, 3\ldots)$. As evident from Equation (14), the choice of stub—open or short—depends on the sign of the sum of susceptances ($B_1 + B_2$), with an open stub for a positive value and a shorted stub for a negative value:

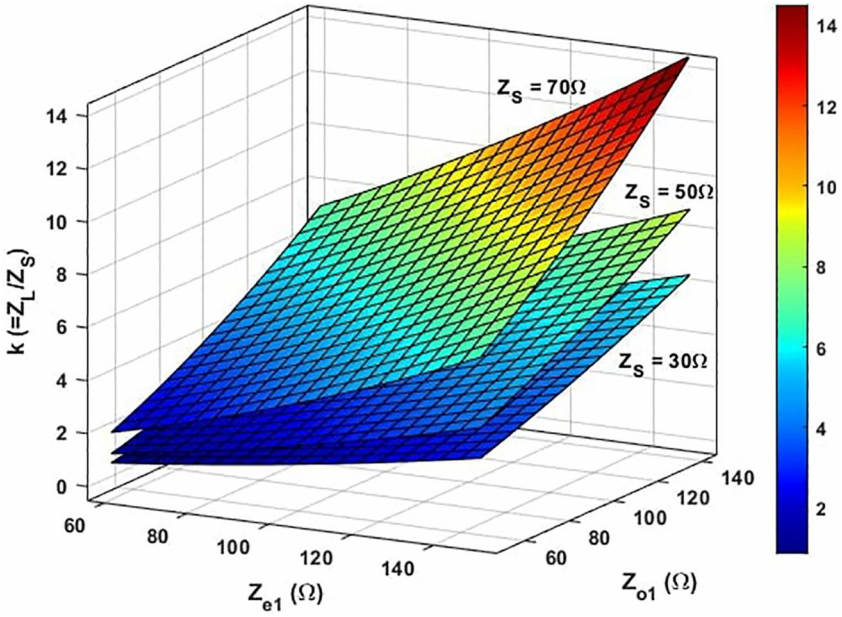

FIGURE 3 Limits of impedance transformation ratio for different values of Z_{e1} and Z_{o1} for different source impedances

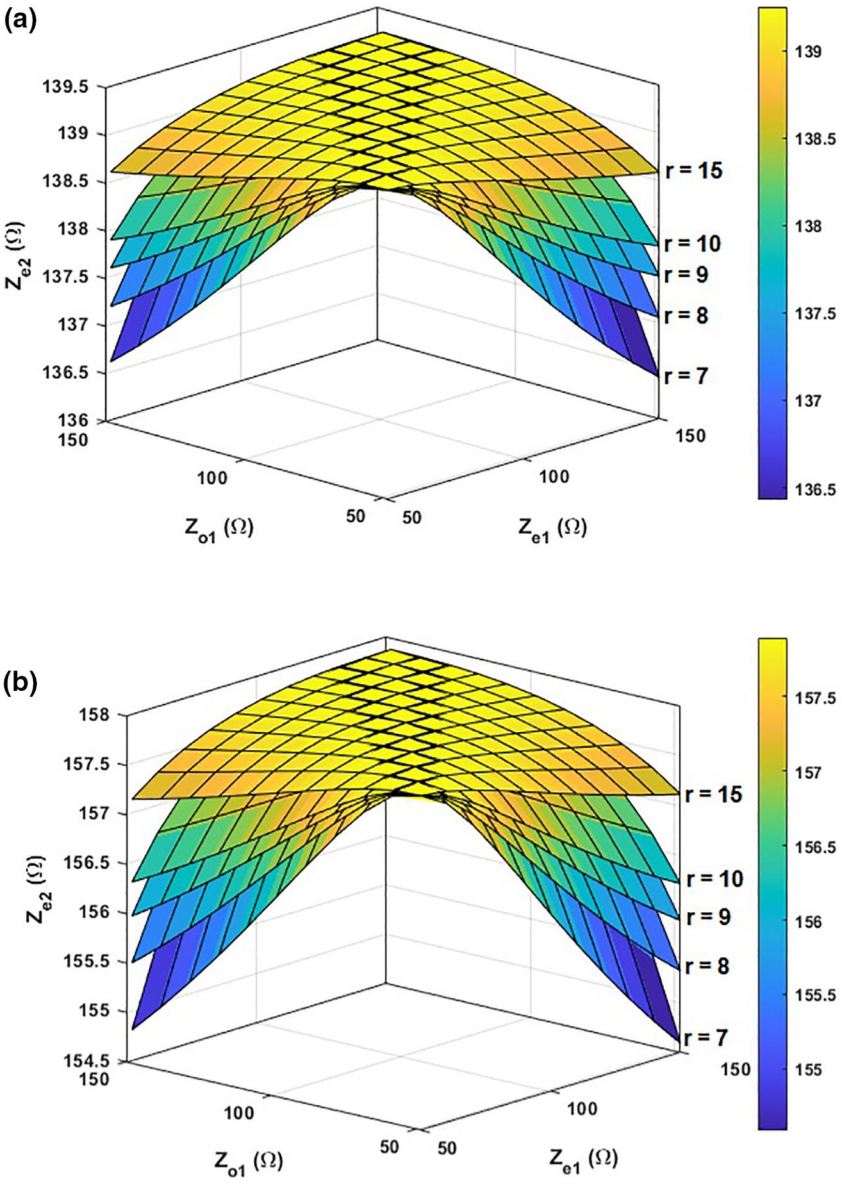

FIGURE 4 Maximum limits of simultaneous extension of frequency ratio and impedance transformation ratio 0 pt 6 pt (a) Maximum possible values of r for $k = 7$, and corresponding line impedances for the set 0 pt 6 pt (b) Maximum possible values of r for $k = 9$, and corresponding line impedances for the set

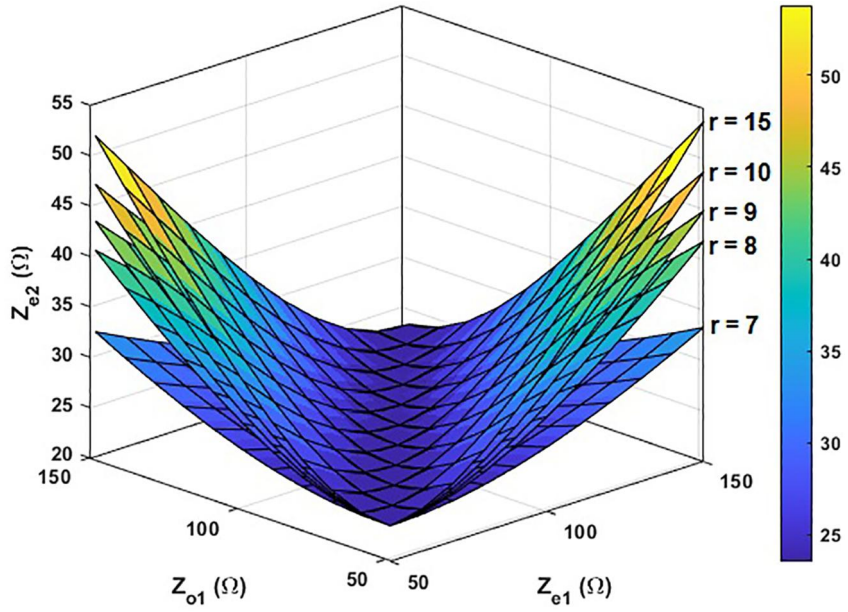

FIGURE 5 Values of r for $k = 0.2$, and corresponding line impedances for the set

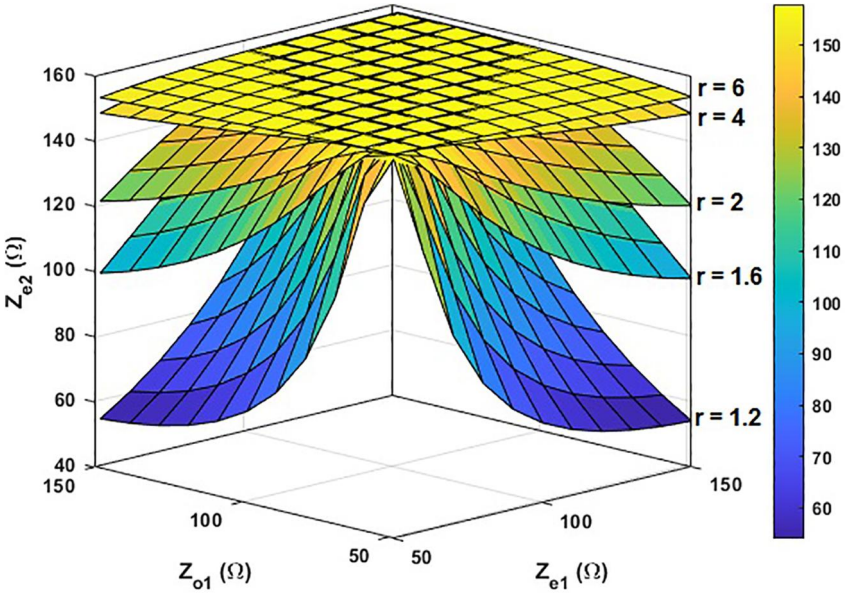

FIGURE 6 Minimum possible values of r for $k = 9$, and corresponding line impedances for the set

$$Z_{OC} = \frac{\tan\theta_S}{(B_1 + B_2)} \tag{14a}$$

$$Z_{SC} = \frac{-1}{(B_1 + B_2)\tan\theta_S} \tag{14b}$$

3 | DESIGN EXAMPLE AND CASE STUDIES

It is imperative to note that the impedance transformation ratio (k) depends directly on the chosen set of [Z_{e1}, Z_{o1}] of the APCL adjoining the load. Figure 3 is a graphical representation of the maximum value of impedance transformation ratio (k) that can be achieved theoretically when varying the design parameters of coupled-line section [Z_{e1}, Z_{o1}] within the fabricable limits. This is shown for different values of source impedances, keeping the case of interstage matching in consideration, where the output impedance of a stage, being the nominal source impedance of the next stage, can be a non-50 Ω real value. However, it is observed that for standard 50 Ω sources, a maximum impedance transformation ratio of 9 is achievable.

While the design parameters of the coupled line [Z_{e1}, Z_{o1}] determine the maximum achievable impedance transformation ratio, the maximum achievable frequency ratio depends mostly on the selection of [Z_{e2}, Z_{o2}] and is studied in Figures 4 through 7. It is observed that with the choice of selection of

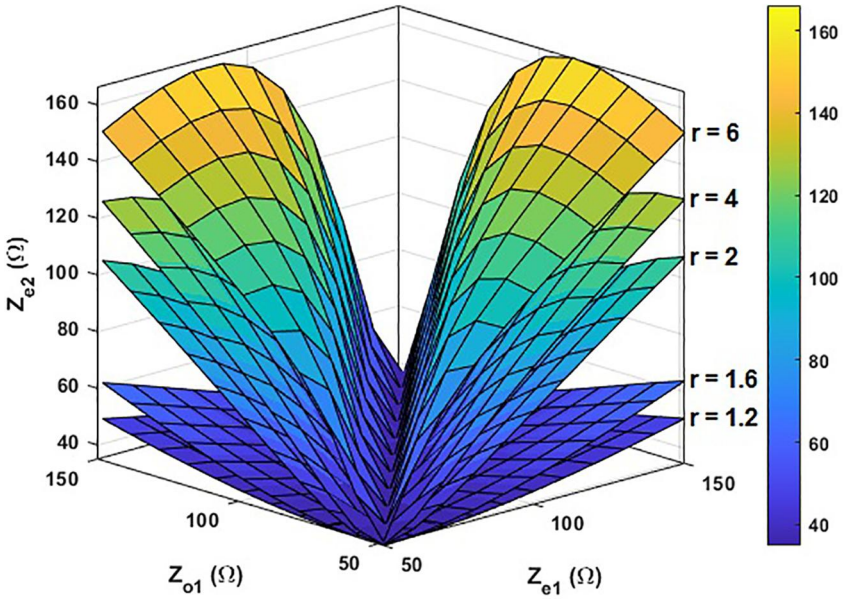

FIGURE 7 Minimum possible values of r for $k = 0.2$, and corresponding line impedances for the set

$[Z_{e1}, Z_{o1}]$ from Figure 3, the impedance surfaces obtained by increasing both transformation ratios (r and k) are within the fabricable limits of [20–160 Ω] in microstrip technology. This directly determines Z_{e2} and hence Z_{o2} from Equation (13). It is worth mentioning that the value of K in Equation (13) should be chosen as around 0.8 or 0.9 for the coupled line to be physically implementable. Figures 4a and 4b illustrate the ability of the network to operate at high impedance transformation ratios at two distantly separate frequency bands (high r). This is clearly denoted by the high impedance surface generated at r = 15 for the two extreme values of k = 7 and k = 9. Figure 5 depicts the lower limits of the achievable impedance transformation ratio for high frequency ratio values. The ability of the proposed network to operate at closely spaced frequencies with contrasting load conditions is illustrated in Figures 6 and 7, where the former portrays a high impedance transformation ability ($k = 9$) at two arbitrary closely spaced frequencies, while the latter depicts the same with severely low loading conditions ($k = 0.2$). From these figures, it is evident that the proposed network is highly flexible in terms of impedance and frequency transformation, with both operating simultaneously. It is also imperative to note that extending any one of the transformation ratios (r or k) towards the upper/lower limit is not detrimental to the other transformation ratio and the matching conditions at the frequencies of interest. Subsequently, few examples have been considered that demonstrate simultaneous enhancement of the frequency ratio and impedance transformation ratio. The cases and corresponding design parameters are listed in Table 1. The values clearly confirm fabrication ability for industrial use. Figure 8 illustrates the simulation results for the case studies from Table 1.

To demonstrate the practical utility of the proposed impedance-matching network, Cases 1, 2, and 5 from Table 1 are fabricated on RO4350 ($\epsilon_r = 3.68$, $1oz\ Cu$) and RO5880

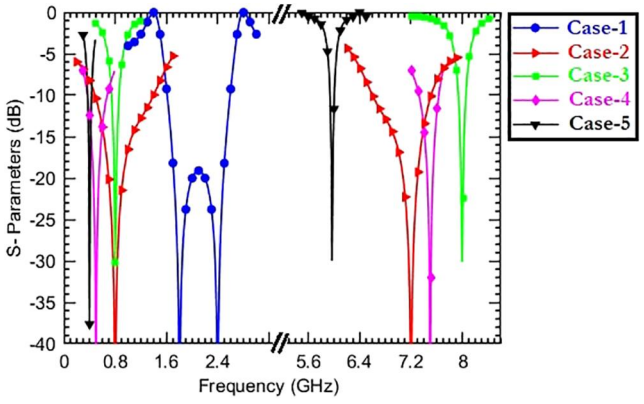

FIGURE 8 Simulation results for the various case studies

($\epsilon_r = 2.2$, $1oz\ Cu$) and measured. Figure 9 illustrates the fabricated prototypes along with the measurement setup for the S parameter measurements. It is evident from Figures 10 through 12 that the measured results achieve perfect matching at the two desired frequencies of interest under the specified loading conditions. It is also worth noting that the proposed design scheme is substrate invariant. As evident from the experiment, a frequency-stable substrate (RO5880) has been chosen for demonstration at higher frequencies, and the measured results show a perfect match at the two desired frequencies ($r = 15$). The circuits are compact in size, thus contributing towards a lower form factor in applications such as an energy harvester. To the best of the authors' knowledge, this is the highest practically implementable frequency ratio obtained to date for a dual-band transformer with simultaneous impedance transformation ratio improvement. The next section describes the application of the proposed impedance-matching topology in designing a TPD.

TABLE 1 Case studies for various frequency and impedance transformation ratios

			Design parameters							
Cases	**r (= f_2/f_1)**	**k (= Z_L/Z_S)**	Z_{e1} (Ω)	Z_{o1} (Ω)	θ_1 (°)	Z_S (Ω)	θ_S (°)	Z_{e2} (Ω)	Z_{o2} (Ω)	θ_2 (°)
1	1.3	6	125	120	77.14	126.71 (SC)	231.42	60	51.8	77.14
2	9	0.3	30	24.7	18	15.95 (OC)	18	36.8	23.7	90
3	10	10	160	156.11	16.36	159.5 (SC)	81.82	160	156.11	81.82
4	15	0.1	23.71	21	11.25	22.27 (OC)	33.75	24.94	23	90
5	15	9	151	149	11.25	160.0 (SC)	78.75	151	149	78.75

Note: (a) The source impedance (Z_S) is kept constant at 50 Ω, and thus, a different k signifies a different load impedance (Z_L). (b) Fundamental frequency f_1 is versatile, signifying matching ability at arbitrary frequencies for the corresponding ratio r.

Abbreviations: OC, open circuit; SC, short circuit.

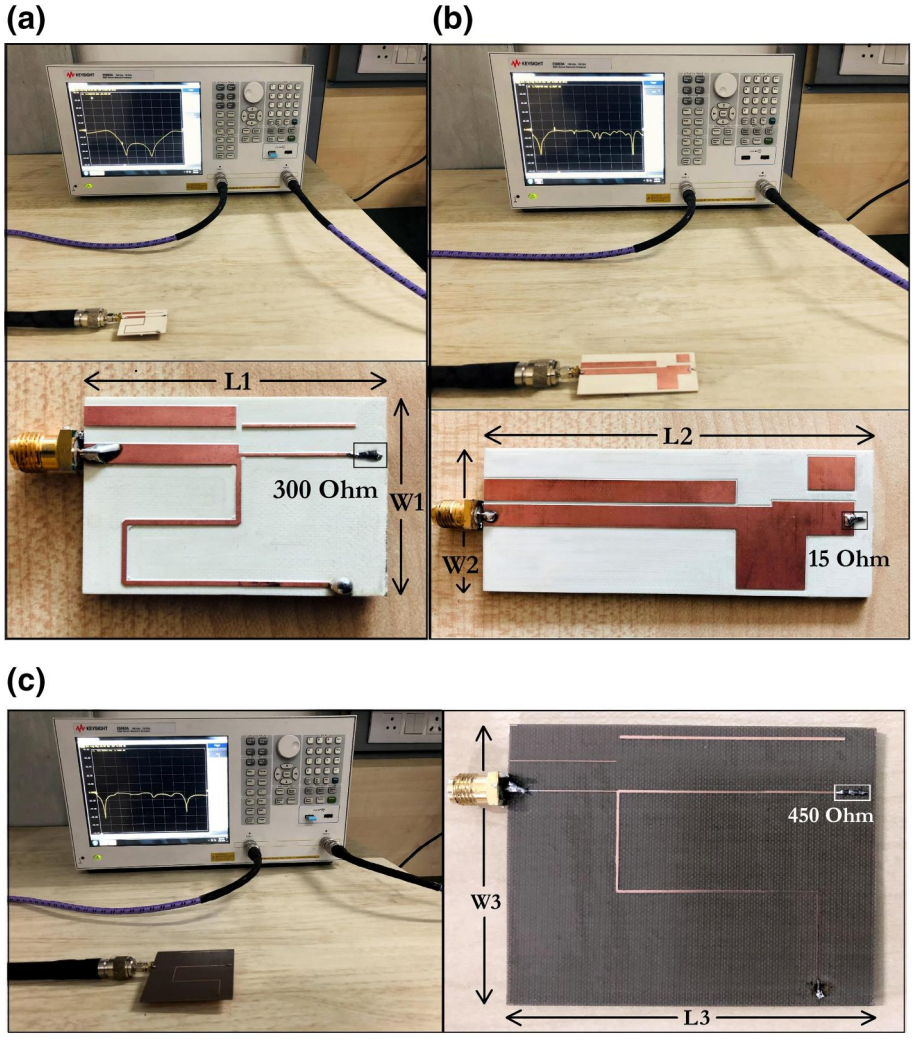

FIGURE 9 Measurement setup for the impedance transformer and their dimensions in terms of guided wavelength (a) For $r = 1.33$, $k = 6.0$, (W1 = $2.65\lambda_g$; $L^1 = 4.12\lambda_g$)@1.8 *GHz* (b) For $r = 9$, $k = 0.3$, (W2 = $1.22\lambda_g$; $L^2 = 3.36\lambda_g$)@800 *MHz* (c) For $r = 15$, $k = 9$, (W3 = $1.25\lambda_g$; $L^3 = 1.35\lambda_g$)@400 *MHz*. Here (L1, W1), (L2, W2), and (L3, W3) are the lengths and widths of the fabricated prototypes in (a), (b), and (c), respectively

4 | APPLICATIONS OF DUAL-BAND T-JUNCTION POWER DIVIDERS

The proposed impedance transformer can be utilised to implement a TPD that divides/combines the power absorbed from radiation at two closely/distantly separated frequency bands. This proves to be suitable in scenarios where isolation is not necessary between the output ports, such as in energy harvesters.

Figure 13 illustrates the proposed equal-split dual-band TPD featuring ultra-high frequency ratios

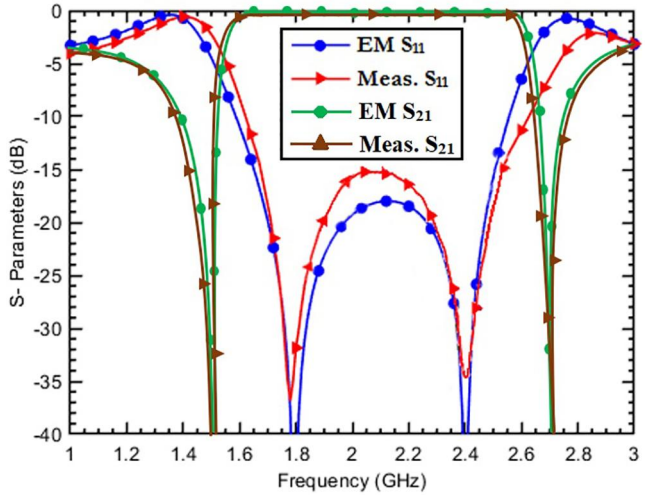

FIGURE 10 Case-1: Measured versus EM results; fractional bandwidth (−15 dB reference) = 19.4%@1.8 *GHz* and 16.6%@2.4 *GHz*

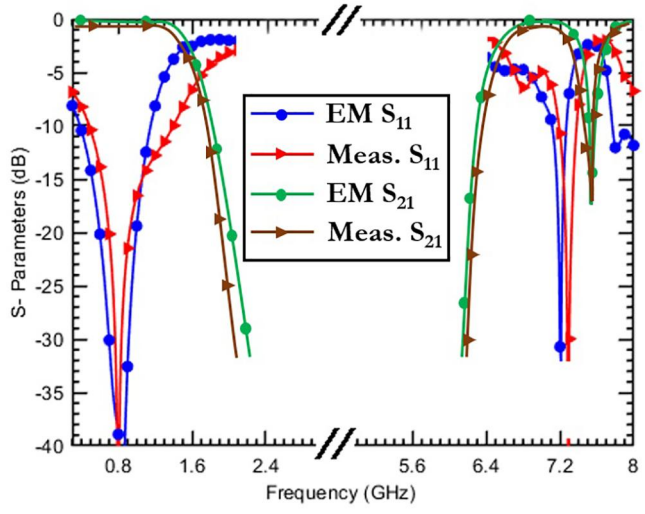

FIGURE 11 Case-2: Measured versus EM results; fractional bandwidth (−10 dB reference) = 125%@800 *MHz* and 5.5%@7.2 *GHz*

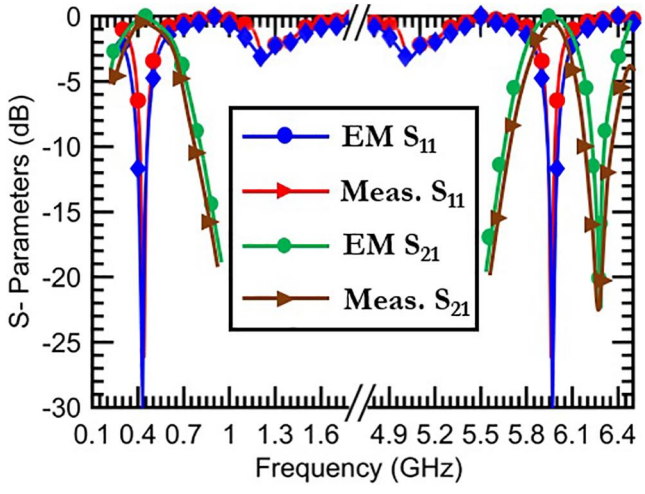

FIGURE 12 Case-5: Measured versus EM results; fractional bandwidth (−10 dB reference) = 50%@400 *MHz* and 5.0%@6.0 *GHz*

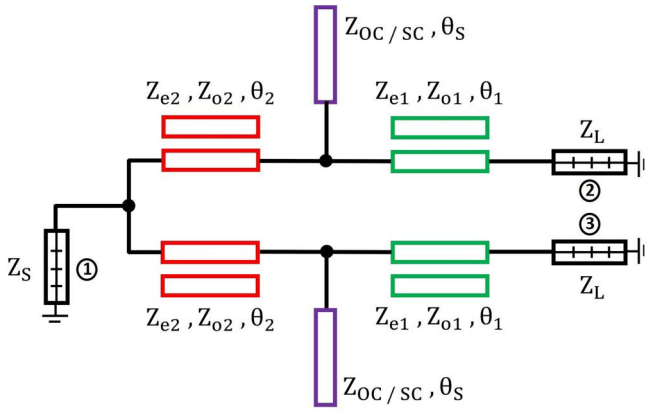

FIGURE 13 Proposed T-junction power divider with ultra-high transformation ratio

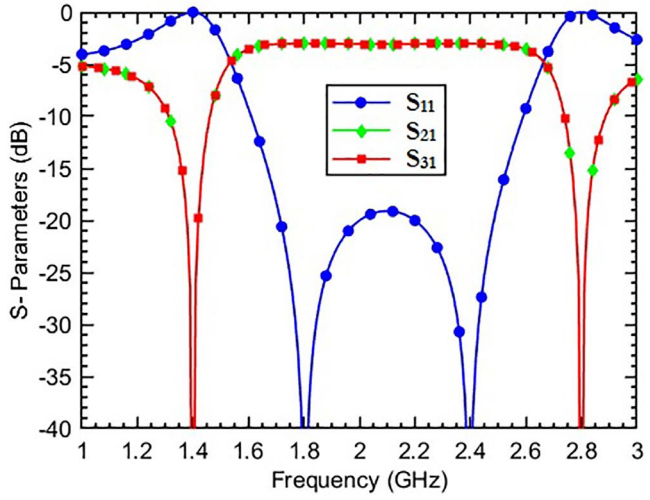

FIGURE 14 S-parameter simulation results of the T-junction power divider (for $k = 0.2$ and $r = 1.33$)

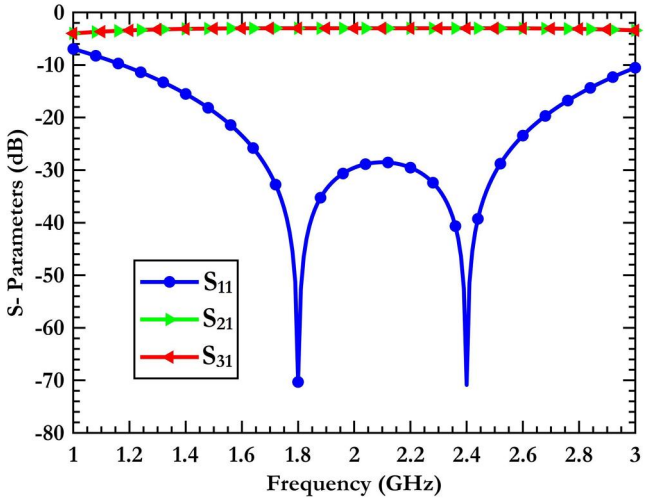

FIGURE 15 S-parameter simulation results of the T-junction power divider (for $k = 5$ and $r = 1.33$)

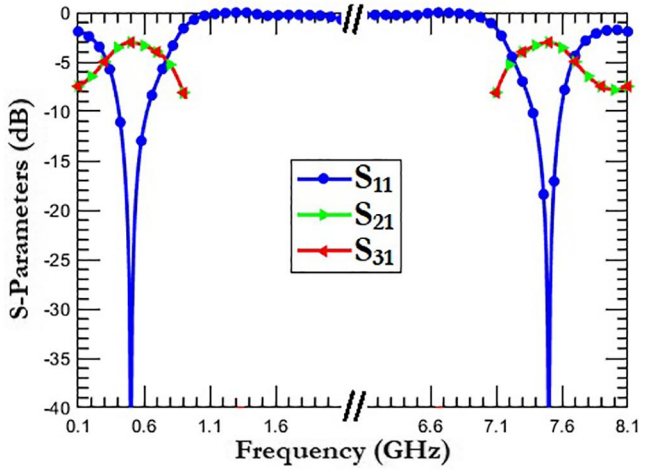

FIGURE 16 S-parameter simulation results of the T-junction power divider (for $k = 0.2$ and $r = 15$)

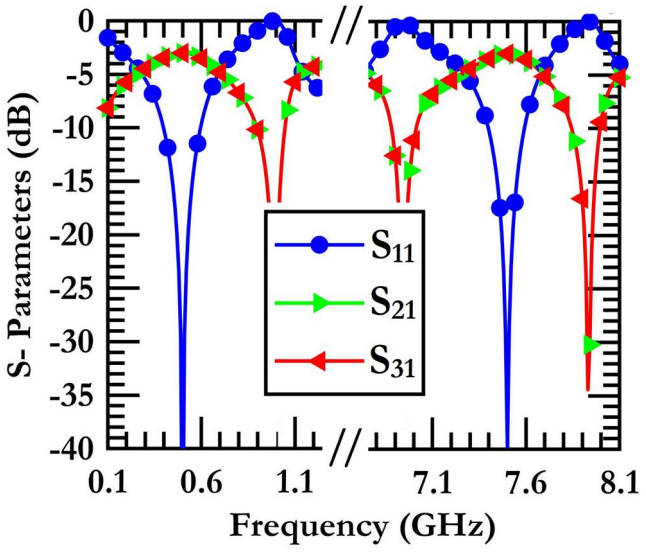

FIGURE 17 S-parameter simulation results of the T-junction power divider (for $k = 5$ and $r = 15$)

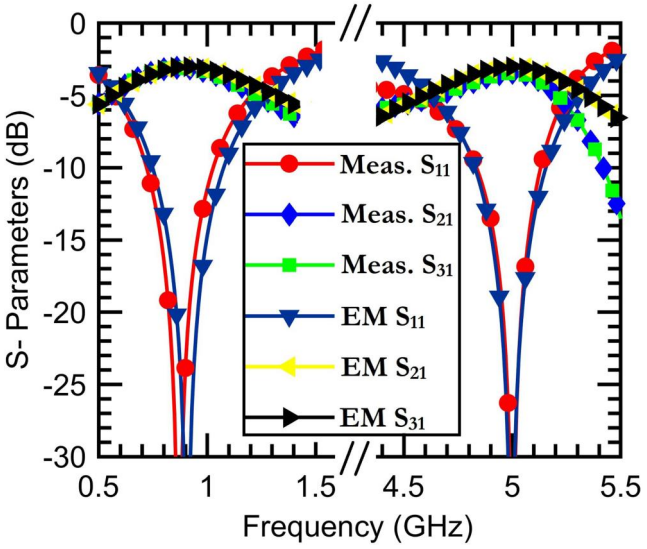

FIGURE 19 Measured results versus Electro-Magnetic (EM) for $r = 6.25$, fractional bandwidth = 61.1%@900 *MHz* and 12%@5.0 *GHz*

developed from the theory discussed above . Conventionally, the ports of a power divider have standard 50 Ω terminations. The design presented here can load the output ports (marked 2 and 3) to a high value. This is done to demonstrate the power division capability, which is augmented with high impedance transformation at extended frequency ratios. As the even- and odd-mode half-circuits are the same in a TPD, the equations to determine the design parameters are the same as those discussed above.

Figures 14 through 17 illustrate different S-parameter responses of the designed TPD under various loading conditions. The output ports are terminated to 250 and 10 Ω, denoting an impedance transformation ratio (k) of 5 and 0.2, respectively, while the frequency ratio (r) is chosen to be as small as 1.33, extending up to 15. This also demonstrates the simultaneous flexibility of impedance

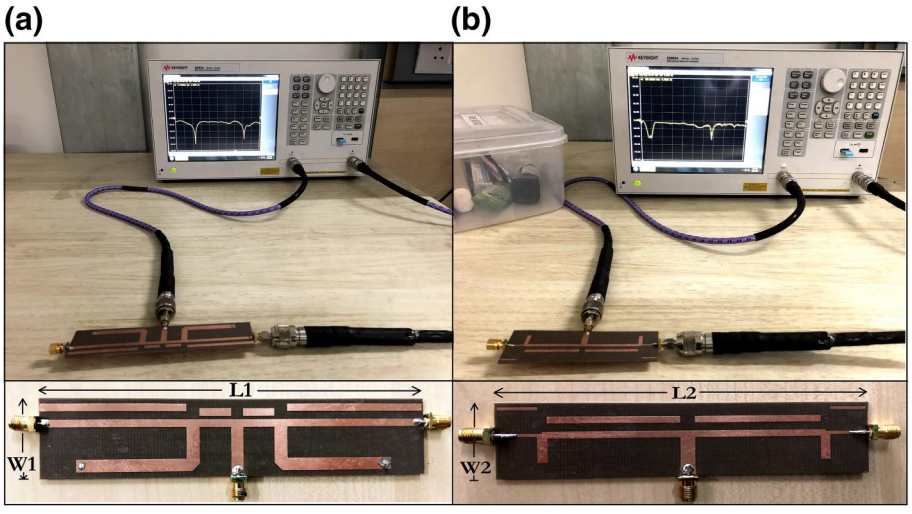

FIGURE 18 Measurement setup for the T-junction power divider (a) For $r = 6.25$, ($W1 = 1.39\lambda_g$; $L^1 = 6.71\lambda_g$)@900 *MHz* (b) For $r = 15$, ($W2 = 0.80\lambda_g$; $L^2 = 2.94\lambda_g$)@500 *MHz*. Here, (L1, W1) and (L2, W2) are the lengths and widths of the fabricated prototypes in (a) and (b), respectively

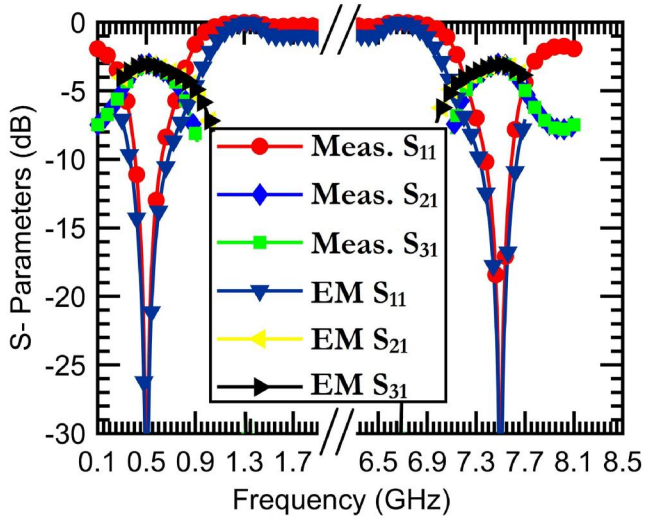

FIGURE 20 Measured results versus Electro-Magnetic (EM) for $r = 15$, fractional bandwidth = 100%@500 *MHz* and 8%@7.5 *GHz*

transformation ratios over a wide range of frequency ratios in both the higher and the lower ranges. It is evident from the case studies that the power divider equally splits the input power in the two uncorrelated frequencies of interest.

To validate the realisation of the proposed TPD, two prototypes, illustrated in Figure 18, have been fabricated on RO5880, and measurements have been performed. It can be inferred from Figures 19 and 20 that the fabricated dividers are a perfect match at the desired frequencies of interest, which are widely apart within the spectrum. The values of the S_{21} and S_{31} parameters are the same at −3.07 dB, and it is also verified that the dividers add power equally from the two ports at the two frequencies. It is noted that while a flexible ultra-high transformation ratio can be achieved, the fractional bandwidth is limited at the upper frequency band. This comes as a trade-off for simultaneous transformation operation of dual-band networks. Although bandwidth increment was not the scope of this research, the proposed design scheme provides commendable bandwidth at the lower band of interest and works perfectly fine for narrowband applications. Table 2 presents a structural and functional comparison of the proposed architecture with a few state-of-the-art designs. It is evident that this design approach advances the state of the art significantly and has the potential to simultaneously enhance the frequency and impedance transformation ratios.

5 | CONCLUSION

A new approach for the development of dual-band impedance-matching networks and TPDs using APCLs has been proposed. The design scheme facilitates a wide range of frequency and impedance transformation ratios. Rigorous mathematical and graphical analyses have been performed to develop a mathematical model for the design process. Based on the design model, three impedance-matching networks and two power divider prototypes have been fabricated and measured under a wide range of loading conditions over a frequency range spanning from 400 MHz to 8.0 GHz. It has also been demonstrated that the proposed model is generic and substrate-independent. Excellent agreement between the simulated and measured results validates the design theory.

TABLE 2 Comparison of a few state-of-the-art designs

Ref. (Year)	Technique used	Frequency ratio (r)	Impedance ratio (k)	Simultaneous r & k transform.	Design flexibility	Design complexity	Approx. Size (λ_g^2) at corresponding Freq.
[11] 2016	Coupled lines	N/A (SB*)	20	No	Low	Complex	N/A
[19] 2019	Coupled lines	3.88	4.0	No	Moderate	Very simple	$(3.64\lambda_g \times 1.6\lambda_g)$@ 900 *MHz*
[20] 2019	Planar TL + coupled line	2–7	0.2–10	No	Low	Moderate	$(1.38\ \lambda_g \times 0.55\lambda_g)$@ 400 *MHz*
[21] 2020	Cross shaped structure	N/A (SB*)	0.1–40	No	Moderate	Simple	$(0.47\lambda_g \times 0.42\lambda_g)$@ 2.4 *GHz*
This work (2021)	**All-pass coupled lines**	**1.2–15**	**0.2–9**	**Yes**	**High**	**Very simple**	$(\mathbf{2.65\lambda_g \times 4.12\lambda_g})$@ 1.8 *GHz*; $(\mathbf{1.25\lambda_g \times 1.35\lambda_g})$ @ 400 *MHz*

Note: λ_g: guided wavelength.

*SB: single-band operation; N/A: not available.

ACKNOWLEDGMENT

This work was supported by the Nazarbayev University CRP Grant 021220CRP0222 and Social Policy Grant.

ORCID

Deepayan Banerjee https://orcid.org/0000-0002-7972-9878

REFERENCES

1. Chow, Y.L., Wan, K.L.: A transformer of one-third Wavelength in two sections - for a frequency and its first harmonic, IEEE Microw Wireless Compon Lett. 12(1), 22–23, (2002)
2. Monzon, C.: A small dual-frequency transformer in two sections, IEEE Trans. Microwave Theory Techn. 51(4), 1157–1161, (2003)
3. Rawat, K., Ghannouchi, F.M.: Dual-band matching technique based on dual-characteristic impedance transformers for dual-band power amplifiers design, IET Microw. Antt. and Prop. 5(14), 1720–1729
4. Chuang, M.L.: Analytical design of dual-band impedance transformer with additional transmission zero, IET Microw. Antt. and Prop. 8(13), p.p. 1120–1126
5. Maktoomi, M.H., Banerjee, D., Hashmi, M.S.: An enhanced frequency-ratio coupled-line dual-frequency Wilkinson power divider, IEEE Trans. on Circ. and Sys.-II: Express Briefs, 65(7), 888–892, (2017)
6. Saxena, A., et al.: Design of compact dual-band matching network with single unequal susceptance cancelation stub, In: IEEE Asia-Pacific Microwave Conference (APMC), 300–302, Kyoto (2018)
7. Rano, D., Banerjee, D., Hashmi, M.S.: A miniaturised three-stage dual-frequency matching network, Proceedings in IEEE International Microwave and RF Conference, 13-16, Ahmedabad (2017)
8. Gong, J.Q., Gao, K., Liang, C.H.: Synthesis of a miniaturised wireless local area network dual-band microstrip Wilkinson power divider through a general three-step optimisation process, IET Microw. Antt. and Prop. 9(12), 1274–1278
9. Wu, Y., et al.: New coupled-line dual-band DC-block transformer for arbitrary complex frequency-dependent load impedance, Microw Opt Technol Lett. 54(1) 139–142, (2012)
10. Manoochehri, O., Asoodeh, A., Forooraghi, K.: Π-Model dual-band impedance transformer for unequal complex impedance loads, IEEE Microw Wireless Compon Lett. 25(4), 238–240, (2015)
11. Wu, Q.S., Zhu, L.: Short-ended coupled-line impedance transformers with ultrahigh transforming ratio and bandpass selectivity suitable for large load impedances, IEEE Trans. Compon., Packag. Manufact. Technol. 6(5), 767–774, (2016)
12. Saxena, A., et al.: Design of π-structure dual-band matching network with unequal susceptance cancelation stubs, Proceedings in IEEE International Microwave and RF Conference, 1-3, Kolkata (2017)
13. Chuang, M.L., Wu, M.T.: General dual-band impedance transformer with a selectable transmission zero, IEEE Trans. Compon., Packag. Manufact. Technol. 6(7), 1113–1119, (2016)
14. Chuang, M.L., Wu, M.T.: Transmission zero embedded dual-band impedance transformer with three shunt stubs, IEEE Microw Wireless Compon Lett. 27(9) 788–790, (2017)
15. Saxena, A., et al.: A dual-band impedance transfomer for matching frequency dependent complex source and load impedances, Proceedings in Conference on Ph.D. Research in Microelectrics and Electronics (PRIME), 173–176, Laussane (2019)
16. Wang, X., Ma, Z., Ohira, M.: Dual-band design theory for dual transmission-line transformer, IEEE Microw Wireless Compon Lett. 27(9) 782–784, (2017)
17. Jiao, L., et al.: Multiband DC-block impedance transformer for extreme complex impedances. Electron Lett. 54(2), 105–107 (2018)
18. Banerjee, D., et al.: A compact dual-band impedance matching network based on all-pass coupled lines. In: Proceedings on IEEE 61st International Midwest Symposium on Circuits and Systems (MWSCAS). Canada (2018)
19. Banerjee, D., Saxena, A., Hashmi, M.S.: A novel design of a bandwidth enhanced dual-band impedance matching network with coupled line wave slowing. In: Proceedings on IEEE 69th Electronic Components and Technology Conference (ECTC). Las Vegas (2019)
20. Gupta, R., et al.: Dual-frequency impedance transformer with ultra- high impedance transformation. In: IEEE Asia-Pacific Microelectrics Conference. Singapore (2019)
21. Zhu, H.X., et al.: Realization of extremely high and low impedance transforming ratios using cross-shaped impedance transformer, IEEE Trans. Circuits Syst. II, 67(7), 1189–1193, (2020)
22. Pozar, D.M.: Microwave Engineering, John Wiley and Sons, 4th ed, pp. 426–430

How to cite this article: Banerjee, D., Hashmi, M., Ghannouchi, F.: Flexible ultra-high transformation ratio-based dual-band impedance transformer and its applications in a T-junction power divider. IET Microw. Antennas Propag. 15(12), 1553–1563 (2021). https://doi.org/10.1049/mia2.12138